Physica Scripta

PAPER

# Electronic, optical, and thermoelectric properties of vacancy-ordered double perovskite $K_2SnX_6$ (X = Cl, Br, I) from first-principle calculations

RECEIVED
3 October 2023

REVISED
15 December 2023

ACCEPTED FOR PUBLICATION
4 January 2024

PUBLISHED
5 February 2024

**A Zikem**[1,2,3], **H Baaziz**[2,3], **T Ghellab**[2,3], **Z Charifi**[2,3] and **F Soyalp**[4]

[1] National School of Built and Ground Works Engineering, B.P. 32, Kouba, Algiers, Algeria
[2] Laboratory of Physics and Chemistry of Materials, University of M'sila, Algeria
[3] Department of Physics, Faculty of Science, University of M'sila, 28000, M'sila, Algeria
[4] Theoretical Physics Research Laboratory, Department of Mathematics and Science, Faculty of Education, Yüzüncü Yıl University, Tuşba Van, 65080, Turkey

**E-mail:** baaziz_hakim@yahoo.fr and hakim.baaziz@univ-msila.dz

**Keywords:** vacancy ordered double perovskites, solar cell, figure of merit, seebeck coefficient, power factor

## Abstract

The present study explores the structural, optoelectronic, and thermoelectric properties of potassium tin halide vacancy-ordered double perovskites $K_2SnX_6$ (X = Cl, Br, and I) in their stable monoclinic phase. Our study uses first-principles calculations based on density functional theory (DFT). Electronic band structures reveal direct band gaps for $K_2SnCl_6$ and $K_2SnBr_6$, while $K_2SnI_6$ exhibits an indirect band gap. Theoretical computations utilising the modified Becke-Johnson potential (mBJ-GGA) demonstrate that the optical band gaps of $K_2SnCl_6$, $K_2SnBr_6$, and $K_2SnI_6$ decrease in the following order: 2.581 eV, 1.707 eV, and 4.126 eV, respectively. These values render the materials suitable for photovoltaic applications. Analysis of dielectric functions, absorption coefficients, and refractive indices demonstrates their potential as light-absorbing materials. We evaluate the thermoelectric properties, including electronic and lattice thermal conductivities, Seebeck coefficients, and power factors, which lead to favorable thermoelectric performance. The maximum figure of merit (ZT) values of 0.58, 0.69, and 0.50 are achieved for $K_2SnCl_6$, $K_2SnBr_6$, and $K_2SnI_6$, respectively, at 500 K. These findings highlight the potential of these materials for applications in solar cells and thermoelectric devices, emphasising their effectiveness at elevated temperatures.

## 1. Introduction

The scientific community is concerned about discovering alternative power generation mechanisms because of the world's escalating energy consumption. Solar cells serve a significant role in the use of renewable energy. On the other hand, thermoelectricity has become a prominent field of study for those seeking an effective non-conventional power generation mechanism. Finding more effective materials with appropriate optoelectronic and thermoelectric properties for power generation has enormous potential.

In the field of optoelectronics, since 2009, researchers have given perovskite solar cells a lot of attention due to their exceptional power conversion efficiency, low cost, and straightforward manufacturing procedure [1–4].

Hybrid organic-inorganic Pb-based halide perovskites with the prototype material $CH_3NH_3PbI_3$ have been on the rise (the certified power conversion efficiency of perovskite solar cells has reached 25.2%). However, two challenges presently stand in the way of the commercialization of large-scale devices: material instability [5, 6] and Pb-related environmental toxicity. The search for novel, stable, Pb-free perovskites is presently generating a lot of research attention [7].

In 2014 [8], Lee *et al* showed that cesium tin (IV) iodide ($Cs_2SnI_6$) has optical and electrical properties that make it useful for photovoltaics. This work sparked new interest in the vacancy-ordered double perovskite family $A_2BX_6$. The direct optical gap of $Cs_2SnI_6$ is 1.3 eV. Lee *et al* used $Cs_2SnI_6$ to construct a solar cell with a

power conversion efficiency of 7.8 %. Furthermore, according to Chen *et al* [9], $Cs_2TiBr_6$ thin film have outstanding intrinsic and environmental stability, long and balanced carrier-diffusion lengths, and a suitable bandgap of 1.8 eV. They also asserted that the initial $Cs_2TiBr_6$ thin films-based perovskite solar cells exhibited a power conversion efficiency of 3.3% [9]. Due to their acceptable optical bandgaps and good stability, $Cs_2TeI_6$ [10], $Cs_2PdBr_6$ [11], and $Cs_2TiBr_6$ [12] are also regarded as potential perovskite materials. However, the earth's crust has limited availability of cesium despite its benefits.

In the realm of thermoelectronics, thermoelectric generators (TEGs) have the potential to extract usable energy from numerous sources, such as industrial operations, power production, and transportation systems. Considerable study has been undertaken on many types of thermoelectric materials, including tin selenide [13], chalcogenides [14–16], half-Heusler alloys [17, 18], Zintl phases [19], perovskites [20–22], and additional materials [23–25]. However, high operating temperatures, cost per watt, and structural complexity have hindered the widespread industrial application of these materials, despite significant progress in improving their efficiency.

The focus then shifts to halide perovskites, which have gained interest because of their advantageous electronic and phononic transport features [26–28]. Theoretical studies have shown that they have very low lattice thermal conductivity [28–31] and strong Seebeck coefficients [32]. However, the fact that lead is poisonous and that $CsMX_3$ (M = Pb, Sn, and X = halide) is structurally unstable in air are big problems that make it hard to use them commercially.

Vacancy-ordered double perovskites have been getting a lot of attention lately because they are better than lead halide perovskites in a number of ways, such as being stable, scalable, and non-toxic [33]. Their tuneable band gaps, long carrier diffusion lengths, good stability in air [34], and flat band structure [35] make them suitable for efficient thermoelectric power production. Various researchers have studied individual compounds within the vacancy-ordered double perovskite family, such as $Cs_2GeCl/Br_6$ [36], $Cs_2SnI_6$, $Rb_2SnI_6$ [37], $K_2OsCl_6$, $K_2OsBr_6$ [38], and $Cs_2NbI_6$ [39], and have reported promising thermoelectric capabilities based on experimental evidence or theoretical calculations.

The $K_2SnX_6$ (X = I, Br, and Cl) vacancy-ordered double perovskite compounds, belonging to the $K_2PtCl_6$-type category, have not been thoroughly explored in terms of thermoelectric, optoelectronic, and related properties. First reported in 1970, only a few investigations had focused on the structural properties of $K_2SnBr_6$ and $K_2SnCl_6$ [40, 41]. Notably, there is a lack of investigation into the thermoelectric and related applications of these compounds, both experimentally and theoretically. Therefore, further investigation is necessary for the potassium tin halide vacancy-ordered double perovskites $K_2SnX_6$ (X = I, Br, and Cl).

This study aims to fill this gap by presenting crucial thermoelectric and optoelectronic parameters for vacancy-ordered double perovskites $K_2SnX_6$ (X = I, Br, and Cl). These parameters include thermal conductivity, electrical conductivity, power factor (PF), Seebeck coefficient, figure of merit, dielectric function, absorption coefficient, reflectivity, refractive index, and optical conductivity. We employ the classical Boltzmann transport theory for these calculations. Additionally, various other important parameters, such as structural, thermal, and band-related characteristics, are computed using the full potential linearized method based on density functional theory. These calculations are expected to pave the way for further research on $K_2SnX_6$ (X = I, Br, and Cl) perovskites. The ultimate goal is to encourage future industrial applications of these compounds.

## 2. Computational methods

One of the best-known methodologies for determining the structural and optoelectronic characteristics of crystalline materials is density functional theory (DFT). The ground-state structural properties of the compounds are estimated by optimising and relaxing the unit cell design. Optimised structural parameters are utilised to compute the electronic, optical, and thermoelectric properties of the compound. In this work, all calculations were done using first-principle methodologies, the Kohn-Sham equation is solved iteratively using the Wein2k [42] algorithm and other integrated simulation tools. Generalised gradient approximation (GGA) is employed [43, 44], and the utilisation of the modified Becke-Johnson potential is employed. (mBJ) [45]. Additionally, muffin-tin spheres are taken into account to enclose the researched components of double perovskites. To achieve the desired behaviour of atomic-like waves inside the spheres and wave-like behaviour outside, the LAPW (linearized augmented-plane wave) technique is utilised with a base set. After a convergence test, the value of $R_{MT}xK_{max} = 9$ is taken into consideration. Regarding the atomic and plane wave cut-offs, it is important to consider their significance in the context of the subject matter. The utilisation of a reduced Brillouin zone (BZ) approach enables the replication of the crystal structure within the confines of regular periodic boundary conditions. A dense grid consisting of 1100 k-points is chosen for the purpose of integrating across the Brillouin zone. The self-consistent termination of iterations occurs when the convergence criterion of

0.0001 e for charge and 0.000001 Ry for energy is satisfied. We employed a total of 10,000 k-points to ascertain the optical properties. We computed and examined the transport characteristics using the BoltzTrap [46].

## 3. Results and discussion

### 3.1. Structural description

It is hypothesised that vacancy-ordered double perovskites $K_2SnX_6$ (X = Cl, Br, and I) experience a phase change from a cubic phase with the (*Fm3m*) space group to a tetragonal phase with the (*P4/mnc*) space group, and finally a transition to a monoclinic ($P2_1/n$) phase when the temperature increases [40, 41]. Figures 1(a)–(c) illustrate the structures of several phases. The current investigation focused on the optimisation of the crystal structures of the compounds $K_2SnX_6$ (where X represents the halogens Cl, Br, and I) that exhibit cubic, tetragonal, and monoclinic crystal structures in their respective phases. This optimisation was carried out using the PBEsol-GGA functional.

In the initial stage, the $K_2SnX_6$ (X = Cl, Br, and I) compounds undergo complete relaxation through the implementation of force optimisation. Energy is represented in terms of volume. After that, we adjust the relationship between volume and energy points to conform to Murnaghan's equation of state [47]. Subsequently, the optimised lattice parameters, bulk modulus, and pressure derivative of the bulk modulus were calculated based on the aforementioned fitting procedure. Table 1 presents the resulting values. Figure 2 presents the graphs depicting the optimised relationship between energy and volume. The anticipated equilibrium lattice parameters are consistent with the available experimental and computational evidence [40, 41], and [48].

The lattice parameters of $K_2SnX_6$ (X = Cl, Br, and I) increase from Cl to Br to I with a decrease in the compressibility modulus *B*. This happens because the combination of larger lattice constants and higher atomic numbers leads to lower material density. Interestingly, the compressibility modulus *B* remains relatively stable when transitioning from cubic to tetragonal to monoclinic phases for each of these compounds. Upon examining multiple volume optimisation graphs, it becomes evident that the monoclinic phase has the highest level of stability among the three phases. Hence, our investigation will primarily concentrate on the monoclinic phase.

### 3.2. Electronic properties

The band gap is a fundamental characteristic of a material. Calculating the band structure determines the band gap of a material. The band gap serves as a method for evaluating the suitability of materials in relation to their prospective use in solar power cells along with other optoelectronic equipment. We determined the band structures of $K_2SnX_6$ (where X represents Cl, Br, or I) using the PBEsol-GGA functional [43, 44]. We also employed the modified Becke-Johnson potential (mBJ) [45]. Figure 3 depicts the profiles of the band structures. The band structures of the three compounds were computed using a selected k-path of Z-C-D-Γ-Y-A-Γ-E within the Brillouin zone. Table 2 presents the estimated bandgaps alongside other calculated data for comparison. With values of 4.126 eV for $K_2SnCl_6$, 2.581 eV for $K_2SnBr_6$, and 1.707 eV for $K_2SnI_6$, the band gaps found with the mBJ-GGA potential show a decreasing trend. The calculated band gaps of $K_2SnX_6$ (X = Cl, Br, and I) exhibit considerable importance for future investigations because of their agreement with the theoretical band gaps [48] of 4.04 eV and 2.57 eV to 1.16 eV, respectively. The band gaps of $K_2SnX_6$ (X = Cl, Br, and I) exhibit favourable characteristics for implementation in single-junction and tandem photovoltaic cells, as well as various other optoelectronic uses. The valence band maximum (VBM) and conduction band minimum (CBM) of $K_2SnCl_6$ and $K_2SnBr_6$ are located at the identical high-symmetry special point Γ. This observation establishes that $K_2SnCl_6$ and $K_2SnBr_6$ possess the characteristic of being direct band gap semiconductors. Whereas, for $K_2SnI_6$ have an indirect band gap between CBM at Γ point and VBM at Y point of the Brillouin Zone.

We determined the total and partial density of states (DOS) for the three compounds under investigation using the mBJ-PBEsol-GGA functional. This analysis was conducted in order to gain a deeper understanding of the intricate electronic characteristics of these compounds, as depicted in figures 4(a)–(c). The partial density of states (DOS) of $K_2SnCl_6$, $K_2SnBr_6$, and $K_2SnI_6$ exhibit certain shared properties. The valence band maximum (VBM) of the three compounds is mostly influenced by the *p* states of the halogen atoms (namely, Cl-*3p*, Br-*4p*, and I-*5p*). Conversely, the conduction band minimum (CBM) is predominantly composed of the s states of tin along with the *p* states of the halogen atoms. Furthermore, it is evident that the presence of potassium has a negligible impact on both the conduction band minimum (CBM) and valence band maximum (VBM).

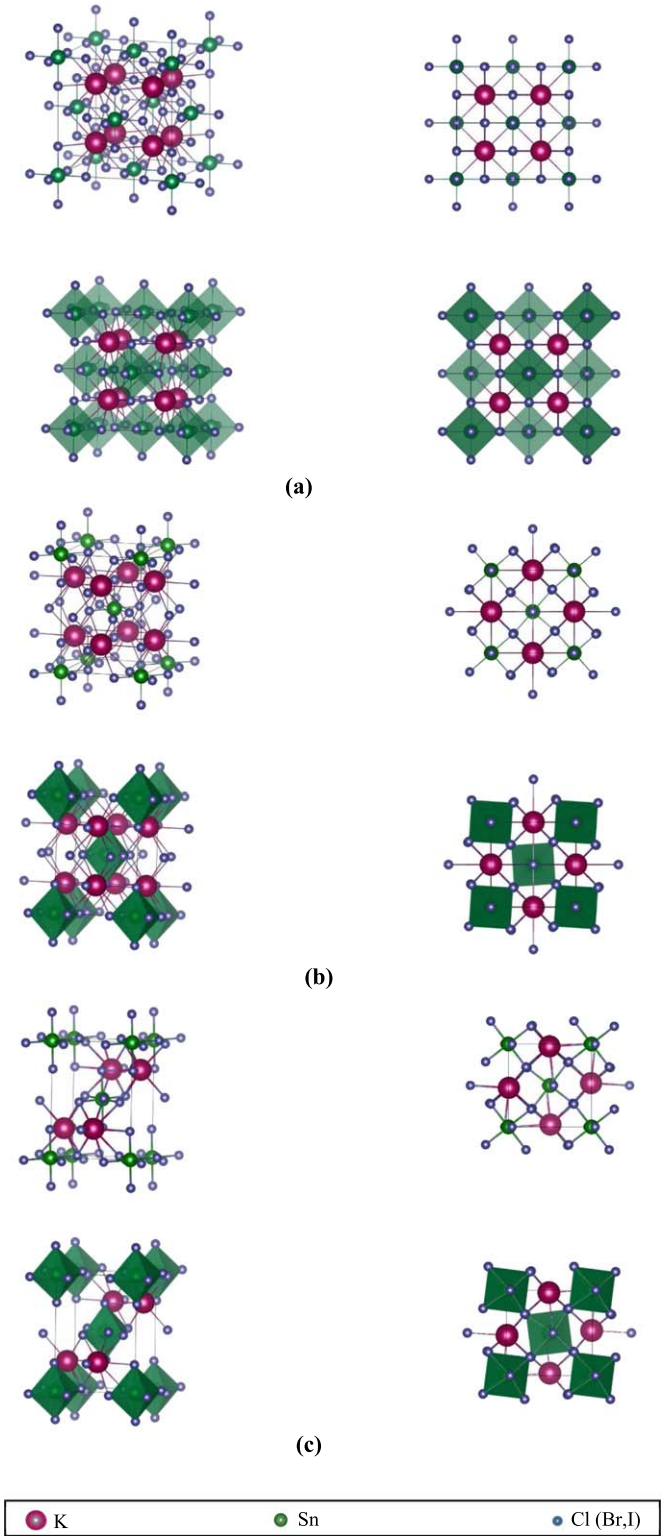


**Figure 1.** The crystal structure and the polyhedral structure of $K_2SnX_6$:(X = Cl, Br, I) (a) cubic, (b) tetragonal, (c) monoclinic.

### 3.3. Optical properties

To assess the viability of $K_2SnX_6$ (X = Cl, Br, I) compounds as light-absorbing materials, we conducted an analysis of various optical characteristics, encompassing dielectric function ($\varepsilon$), light-absorption coefficients ($\alpha$), refractive index (n), reflectivity coefficient (R), extinction coefficient (k), and the energy associated with the loss function (L), using the PBEsol-GGA functional with and without mBJ correction.

The complex dielectric function explains how a photon interacts with various materials. It determines the linear optical characteristics. The complex dielectric function has the following expression: $\varepsilon = \varepsilon_1 + i\varepsilon_2$. The two constituents, $\varepsilon_1$ and $\varepsilon_2$ represent the real and imaginary components of the dielectric constants, respectively.

**Table 1.** Calculated lattice constants, compared to experimental parameters.

| Materials | Phases | Calculated parameters by GGA-PBEsol | Calculated parameters by GGA-PBE [48] | Experimental parameters [40, 41] |
|---|---|---|---|---|
| $K_2SnCl_6$ | Cubic | $a = 9.9834$ Å<br>B (GPa) = 36.0755<br>B' = 5.0474<br>$V_0$ (Bohr$^3$) = 1678.7077<br>$E_{min}$ (Ryd) = −20288.856533 | $a = 10.02$ Å | $a = 9.99$ Å |
| | Tetragonal | $a$ = b = 7.0599 Å, $c = 9.9963$ Å<br>B (GPa) = 35.7786<br>B' = 4.9392<br>$V_0$ (Bohr$^3$) = 3357.2765<br>$E_{min}$ (Ryd) = − 40577.720090 | $a = b = 7.09$ Å, $c = 10.01$ Å | $a = b = 7.06$ Å, $c = 9.98$ Å |
| | Monoclinic | $a = 7.0399$ Å, $b = 7.0299$ Å,<br>$c = 10.0183$ Å, $\beta = 90.23°$<br>B (GPa) = 36.1102<br>B' = 4.9442<br>$V_0$ (Bohr$^3$) = 3345.7984<br>$E_{min}$ (Ryd) = − 40577.725147 | $a = 7.07$ Å, $b = 7.05$ Å,<br>$c = 10.03$ Å, $\beta = 90.11°$ | $a = 7.02$ Å, $b = 7.01$ Å,<br>$c = 9.99$ Å, $\beta = 90.13°$ |
| $K_2SnBr_6$ | Cubic | $a = 10.5091$ Å<br>B (GPa) = 29.2572<br>B' = 4.9089<br>$V_0$ (Bohr$^3$) = 1958.0934<br>$E_{min}$ (Ryd) = − 46018.066061 | $a = 10.51$ Å | $a = 10.48$ Å |
| | Tetragonal | $a = b = 7.4687$ Å, $c = 10.6268$ Å<br>B (GPa) = 28.3798<br>B' = 5.0768<br>$V_0$ (Bohr$^3$) = 3999.8251<br>$E_{min}$ (Ryd) = − 92036.131139 | $a = b = 7.50$ Å, $c = 10.67$ Å | |
| | Monoclinic | $a = 7.4228$ Å, $b = 7.4328$ Å,<br>$c = 10.6097$ Å, $\beta = 90.42°$<br>B (GPa) = 29.2196<br>B' = 6.0121<br>$V_0$ (Bohr$^3$) = 3950.1665<br>$E_{min}$ (Ryd) = − 92036.172004 | $a = 7.45$ Å, $b = 7.47$ Å,<br>$c = 10.68$ Å, $\beta = 90.17°$ | $a = 7.43$ Å, $b = 7.44$ Å,<br>$c = 10.62$ Å, $\beta = 90.18°$ |
| $K_2SnI_6$ | Cubic | $a = 11.5230$ Å<br>B (GPa) = 20.7168<br>B' = 5.2102<br>$V_0$ (Bohr$^3$) = 2581.2577<br>$E_{min}$ (Ryd) = − 100151.869977 | $a = 11.66$ Å | |
| | Tetragonal | $a = b = 8.1334$ A, $c = 11.5938$ Å<br>B (GPa) = 20.7228<br>B' = 5.4586<br>$V_0$ (Bohr$^3$) = 5175.6526<br>$E_{min}$ (Ryd) = − 200303.744305 | $a = b = 8.25$ Å , $c = 11.76$ Å | |
| | Monoclinic | $a = 8.1866$ Å, $b = 8.2532$ Å,<br>$c = 11.4979$ Å, $\beta = 90.50°$<br>B (GPa) = 20.2292<br>B' = 5.4260<br>$V_0$ (Bohr$^3$) = 5242.4576<br>$E_{min}$ (Ryd) = − 200303.804663 | $a = 8.29$ Å, $b = 8.32$ Å,<br>$c = 11.69$ Å , $\beta = 90.25°$ | |

Figures 5(a) and (b) depict the two parts of the dielectric function for the indicated materials, specifically for energy values ranging from 0 to 5 eV, in the context of optical computations. The plots exhibit essentially indistinguishable trends across all compounds, with the exception of a minor deviation towards lower energy levels when the compounds transition from $K_2SnCl_6$ to $K_2SnBr_6$ to K2$SnI_6$.

The imaginary component of the dielectric function $\varepsilon_2$ determines the magnitude of light absorption in a substance. The energy band gap is the threshold at which absorption initiates in a given material as a result of the electronic transition from the valence band maximum (VBM) to the conduction band minimum (CBM). The optical gaps for $K_2SnCl_6$, $K_2SnBr_6$, and $K_2SnI_6$ were determined to be 4 eV, 2.3 eV, and 1 eV, respectively (mBJ-GGA). The optical bandgaps obtained from the calculations validate the accuracy of the computational methodology employed in this study by aligning with the theoretical bandgaps derived from the band structure

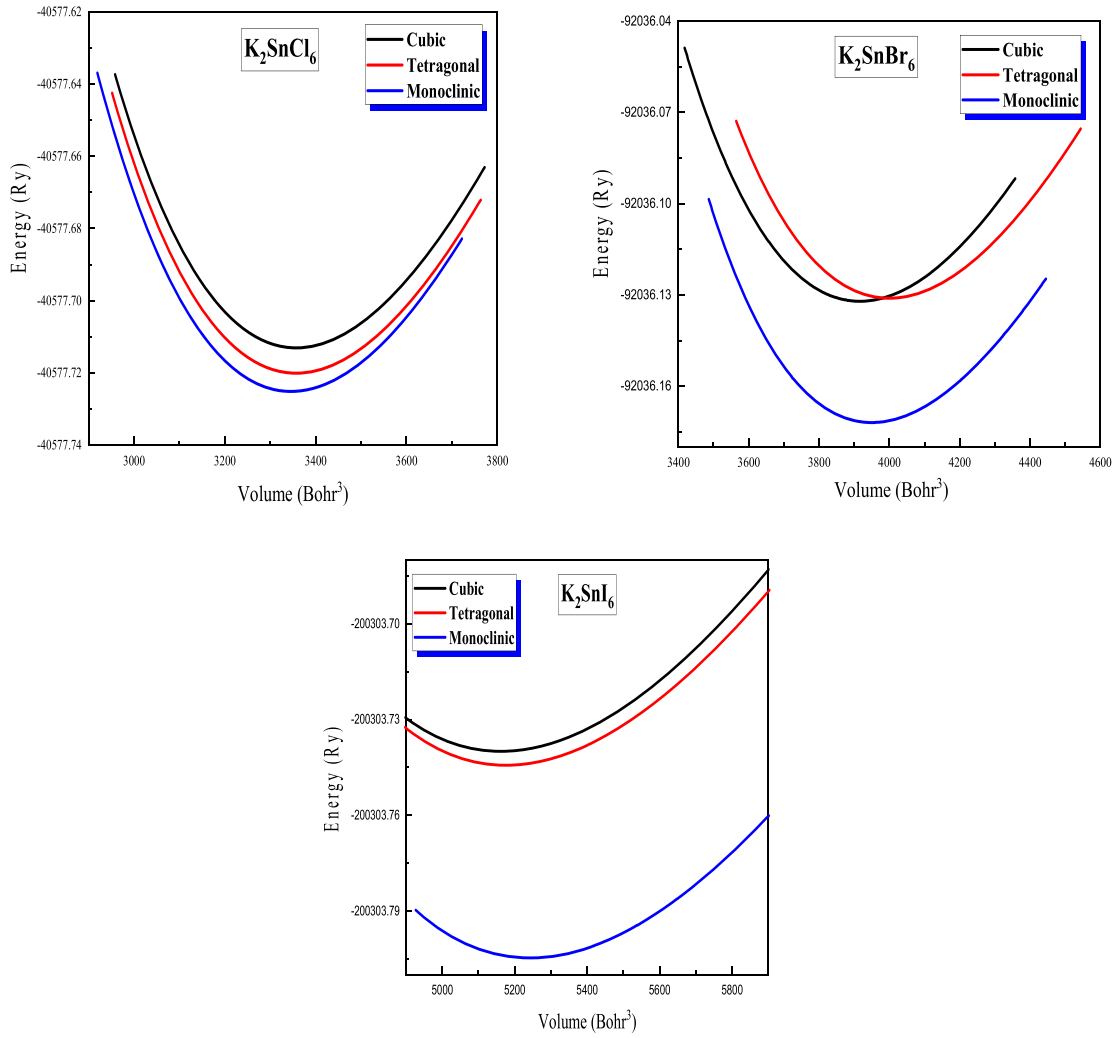


**Figure 2.** Total volume-dependent energy variation of the $K_2SnX_6$ (X = Cl, Br, I) unit cell, for cubic, tetragonal, and monoclinic phases.

analysis. The graph exhibits its peak values for $K_2SnBr_6$ and $K_2SnI_6$ at energy levels of 3.64 eV and 2.38 eV, respectively. Nevertheless, the value of $\varepsilon_2$ remains consistently low for $K_2SnCl_6$. Moreover, it was subsequently shown that the dielectric constants of $K_2SnX_6$ (X = Cl, Br, I) exhibit an increase when the ionic radius of the halogen anion increases. The intensity of $K_2SnI_6$ in the $\varepsilon_2$ spectra is observed to be higher compared to the other elements within the visible range, suggesting a notable level of absorptive activity.

Employing the Kramers-Kronnig transformation, the real component of the dielectric function $\varepsilon_1$ is derived from its imaginary component. The real component $\varepsilon_1$ is a measure of the degree of light polarisation observed as light passes through a material. For $K_2SnCl_6$, $K_2SnBr_6$, and $K_2SnI_6$, the static dielectric constants at the zero frequency limit are $\varepsilon_1(0) = 2.22$, 2.90, and 3.76, respectively. The compounds $K_2SnBr_6$ and $K_2SnI_6$ exhibit enhancements in the magnitude of $\varepsilon_1$ ranging from 3.73 to 4.76. These enhancements occur at energies of 2.97 eV and 1.92 eV for $K_2SnBr_6$ and $K_2SnI_6$, respectively.

Important information for the application prospects can be found in the absorption coefficient ($\alpha$) as shown in figure 5(c). In visible light, it is apparent that as the energy of the photons increases, the intensity of the absorption coefficient for each compound under study increases. Because their band gaps are smaller, $K_2SnI_6$ and $K_2SnBr_6$ absorb visible light better than $K_2SnCl_6$. This means that $K_2SnBr_6$ and $K_2SnI_6$ are better choices as light-absorbing materials for solar cells. $K_2SnCl_6$ may be explored as a potentially viable semiconductor material for tandem solar power generation and various optoelectronic devices due to its favourable light absorption characteristics when subjected to photon energies over 3 eV.

Figure 5(d) depicts the refractive index ($n$), which indicates the degree of transparency or opacity exhibited by the materials. The static refractive index values for $K_2SnCl_6$, $K_2SnBr_6$, and $K_2SnI_6$ are 1.75, 1.98, and 2.23, respectively. Moreover, the apex of $n$ corresponds to an electronic transition from the valence band maximum (VBM) to the conduction band minimum (CBM). The peak for $K_2SnBr_6$ is located at 3 eV, whereas for $K_2SnI_6$, it

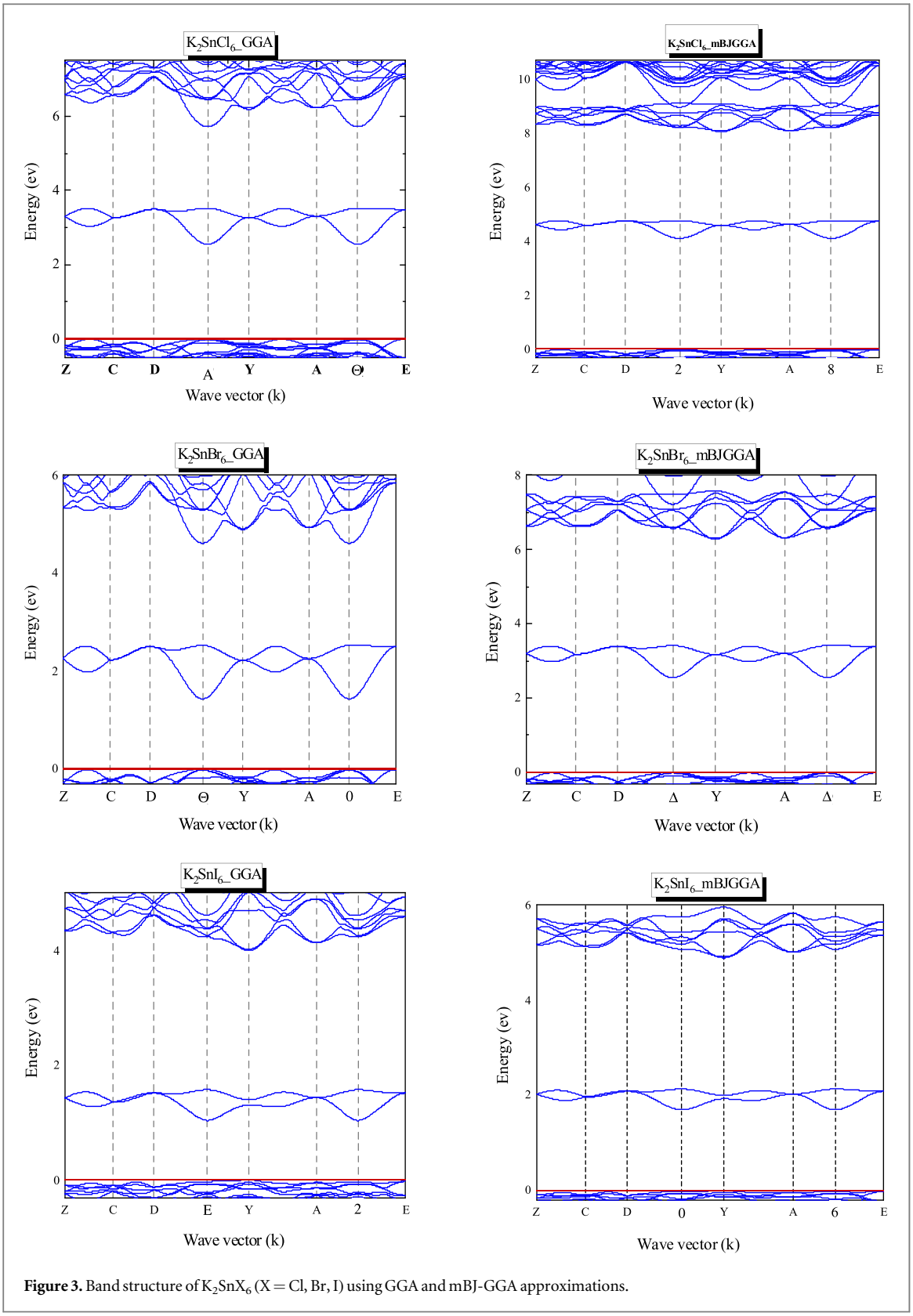


**Figure 3.** Band structure of $K_2SnX_6$ (X = Cl, Br, I) using GGA and mBJ-GGA approximations.

is set at 1.9 eV. These energy levels make them well-suited for solar applications. $K_2SnCl_6$ has a relatively low refractive index within the visible light spectrum. The values of *n* revealed in this study for the vacancy-ordered double perovskite are highly suitable for application in solar cells.

Reflectivity (*R*) is a fundamental optical parameter that quantifies the amount of light reflected from a given surface. Figure 5(e) displays the reflectivity spectra of $K_2SnCl_6$, $K_2SnBr_6$, and $K_2SnI_6$. The compounds are believed to exhibit transparency to photons in visible light due to their reflectivity in the visible spectrum being

**Table 2.** Band gaps Eg calculated using PBEsol-GGA and mBJ- PBEsol-GGA compared to theoretical results.

| Compounds | *Eg* | | |
|---|---|---|---|
| | PBEsol-GGA | mBJ-PBEsol-GGA | Theoretical [48] |
| $K_2SnCl_6$ | 2.577 eV | 4.126 eV | 4.04 eV |
| $K_2SnBr_6$ | 1.465 eV | 2.581 eV | 2.57 eV |
| $K_2SnI_6$ | 1.060 eV | 1.707 eV | 1.16 eV |

below 15%. It is evident from the data presented in figure 5(f) that the variation in the extinction coefficient ($k$) follows a similar pattern to that of the absorption coefficient ($n$).

The energy-loss function (L) is a crucial metric used to characterise the likelihood of light decay as it traverses a material. Figure 5(g) presents the electron energy loss spectrum (L). It is noteworthy that within the measured range, the energy-loss functions have values that are consistently less than 0.04. The energy loss in this study can be considered negligible. It is evident that the extinction coefficient and energy-loss function curves demonstrate similar patterns.

The optical conductivity $\sigma$ encompasses various aspects that elucidate the correlation between the oscillating electric field $E$ and the current density $j$. Figure 5(h) depicts the spectrum of optical conductivity, which displays many peaks, each of which corresponds to transitions between bands.

### 3.4. Thermoelectric properties

In recent times, there has been a growing interest in thermoelectric materials due to their notable ability to convert thermal energy into electrical energy. The evaluation of thermoelectric devices' performance is conducted through the utilisation of the figure of merit, $\boldsymbol{ZT} = \frac{S^2\sigma T}{\kappa}$ [49].

The parameters are the Seebeck coefficient (S), electrical conductivity ($\sigma$), total thermal conductivity ($\kappa$), and absolute Kelvin temperature (T). A large S and $\sigma$ with a small $\kappa$ are characteristics of a good thermoelectric device. The calculation of the figure of merit (ZT) involved the total thermal conductivity $\kappa = \kappa_e + \kappa_L$, which is the sum of the electronic thermal conductivity ($\kappa_e$) and the lattice thermal conductivity ($\kappa_L$).

It is widely believed that thermoelectric materials of high quality possess semiconductor properties characterised by conduction and valence bands that have a flat energy profile [50]. The band structures that we have computed (figure 3) illustrate that $K_2SnCl_6$, $K_2SnBr_6$, and $K_2SnI_6$ exhibit characteristics of direct band gap semiconductors, wherein the conduction and valence bands remain flat. Therefore, it is expected that they will exhibit favourable thermoelectric characteristics. The present study employed the Boltzmann transport theory to ascertain the thermoelectric characteristics. Therefore, (S), ($\sigma$), ($\kappa_e$), and power factor (PF) were determined by employing Boltzmann transport theory through the utilisation of the BoltzTraP code [46]. The relaxation time is consistently maintained at $10^{-14}$ s. We calculated $\kappa_L$ using the Slack equation [51]implemented in the Gibbs code [52, 53].

Figure 6(a) displays the electronic thermal conductivity ($\kappa_e$) at various temperatures. The charge carrier's contribution to heat transfer is represented by $\kappa_e$. It is evident that for the three compounds, their value rises as the temperature increases. Figure 6(b) illustrates the lattice contribution to thermal conductivity ($\kappa_L$) as a function of temperature, as determined by the utilisation of the slack equation [51]. The values of $\kappa_L$ exhibit a decrease as the temperature increases. The observed behaviour of $\kappa_L$ indicates a decrease in phonon heat transmission as temperature rises. Additionally, figure 6(c) illustrates the relationship between temperature and the total heat transfer by charge carriers and phonons ($\kappa$). The thermal conductivity values of $K_2SnCl_6$ decline until reaching 200 K, $\kappa$ ($K_2SnBr_6$) decrease until reaching 250 K, and $\kappa$ ($K_2SnI_6$) decrease until reaching 350 K. After these respective temperatures, the total thermal conductivity ($\kappa$) exhibits a slight increase with rising temperature. This increase is a result of the fact that the number of charge carriers increases with temperature.

Figure 6(d) shows how electrical conductivity ($\sigma$) changes with temperature. The graph shows that when the temperature rises, $\sigma$ increases. The following relationship links $\sigma$ with carrier concentration $n$: $\sigma = ne\mu$. Where $\mu$: is the mobility and $e$ is the electrical charge. The rise in carrier concentration is the cause of the positive temperature dependence of $\sigma$. The low values of conductivity ($\sigma$) observed in $K_2SnI_6$ can be attributed to the limited mobility of charge carriers in the material. This reduced mobility is primarily due to its relatively small bandgap (Eg). When Br and Cl are substituted to I, the bandgaps are greater, which results in an increase in electrical conductivity.

The Seebeck coefficient (S) is calculated and presented in figure 6(e) within the temperature interval ranging from 100 K to 500 K. In the full temperature range, the figure demonstrates that the Seebeck coefficient (S) values for the $K_2SnX_6$ (X = Cl, Br, and I) compounds are positive. This demonstrates that the investigated compounds

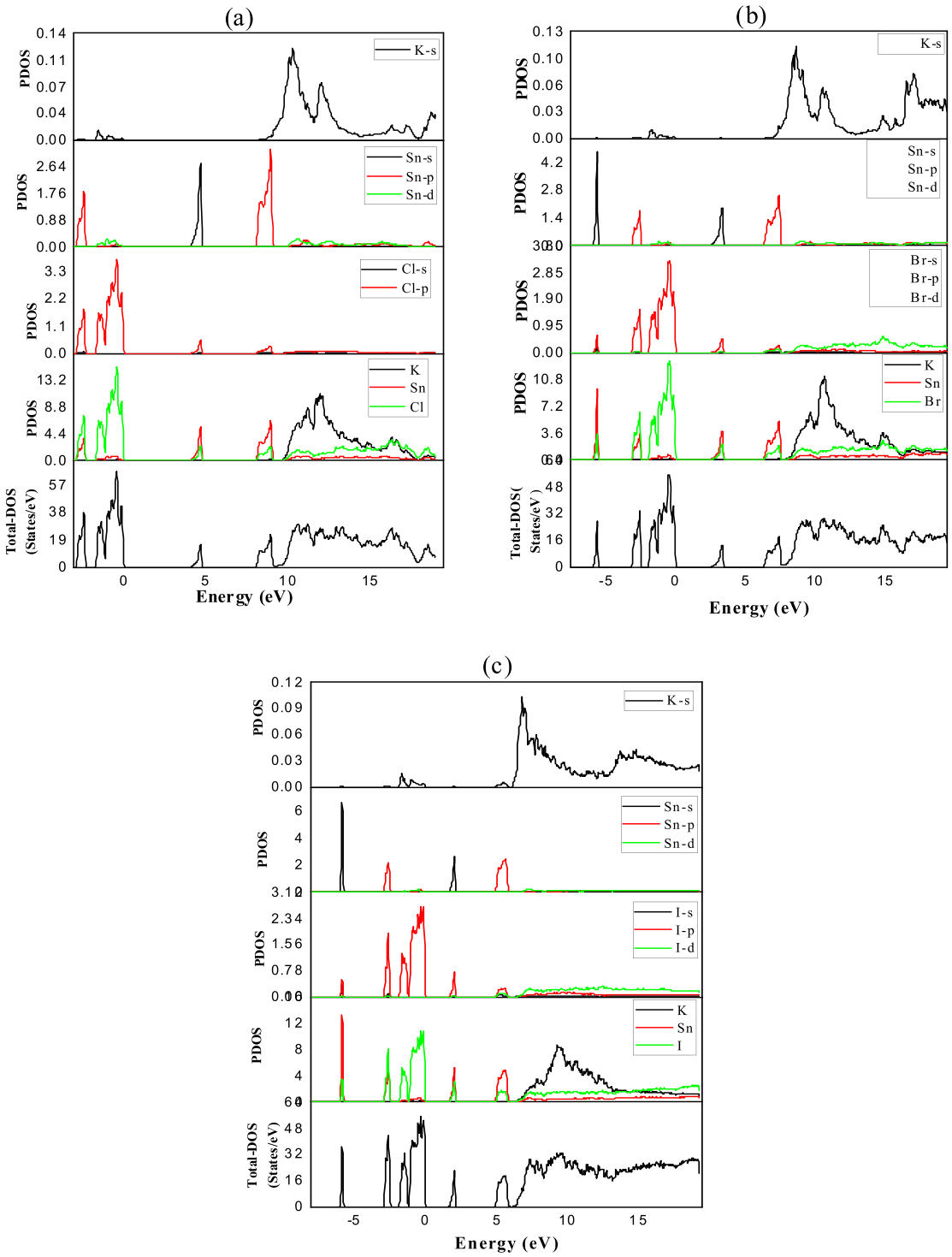


**Figure 4.** Total and partial density of state DOS in the monoclinic phase, calculated by mBJ-GGA functional of: (a) $K_2SnCl_6$, (b) $K_2SnBr_6$, (c) $K_2SnI_6$.

have p-type conductivity. Additionally, the value of S decreases with rising temperature, similarly to other semiconductors.

One important parameter for transport properties is the power factor ($PF = \sigma S^2$). Figure 6(f) depicts how it changes with temperature for $K_2SnX_6$ (X = Cl, Br, and I). PF increases from $\sim 2.5 \times 10^{-4}$ W mK$^{-2}$ (at 50 K) to $\sim 3 \times 10^{-3}$ W mK$^{-2}$ (at 500 K) for $K_2SnCl_6$ and $K_2SnBr_6$, and from $\sim 2.5 \times 10^{-4}$ W mK$^{-2}$ (at 50 K) to $1.5 \times 10^{-3}$ W mK$^{-2}$ (at 500 K) for $K_2SnI_6$. The calculated PF values assure their overall potential as effective thermoelectric materials [36–39].

Figure 6(g) displays the Figure of merit (ZT) variation in terms of temperature. At 500 K, $K_2SnCl_6$, $K_2SnBr_6$, and $K_2SnI_6$ have maximum ZT values of 0.58, 0.69, and 0.50, respectively. In comparison with metal and lead

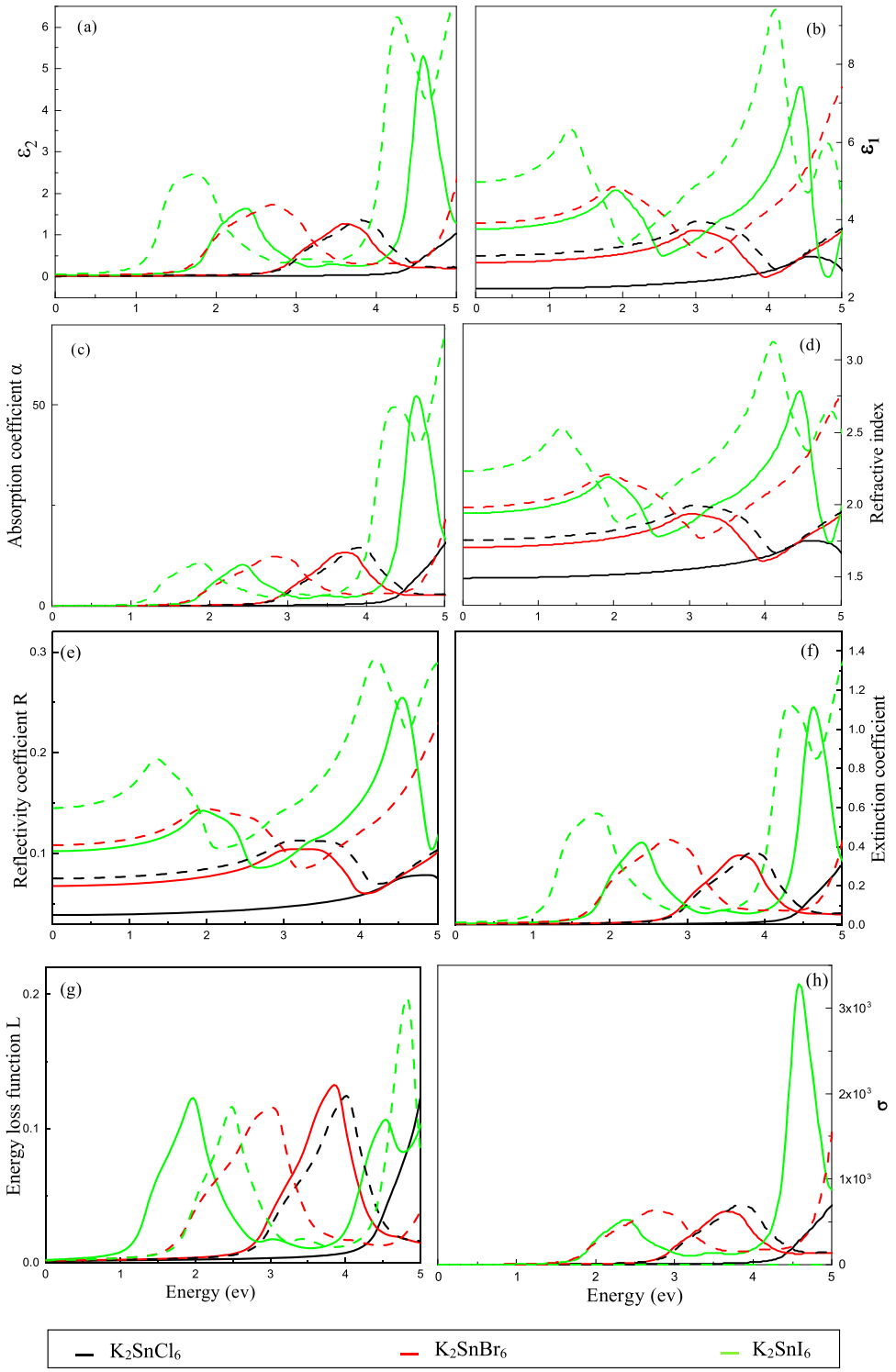


**Figure 5.** The computed optical parameters of $K_2SnX_6$ (X = Cl, Br, I) in monoclinic phase calculated by GGA (dashed lines), mBJ-GGA (solid line) approximations.

halide perovskites [54], these values are significantly high. It is pertinent to mention that the materials under study are more effective for thermoelectric applications at high temperatures.

## 4. Conclusion

The exploration of materials exhibiting excellent optoelectronic and thermoelectric capabilities for the purpose of power generation possesses significant potential. This study aims to examine the structural, optoelectronic, and thermoelectric properties of potassium tin halide vacancy-ordered double perovskites $K_2SnX_6$ (where X

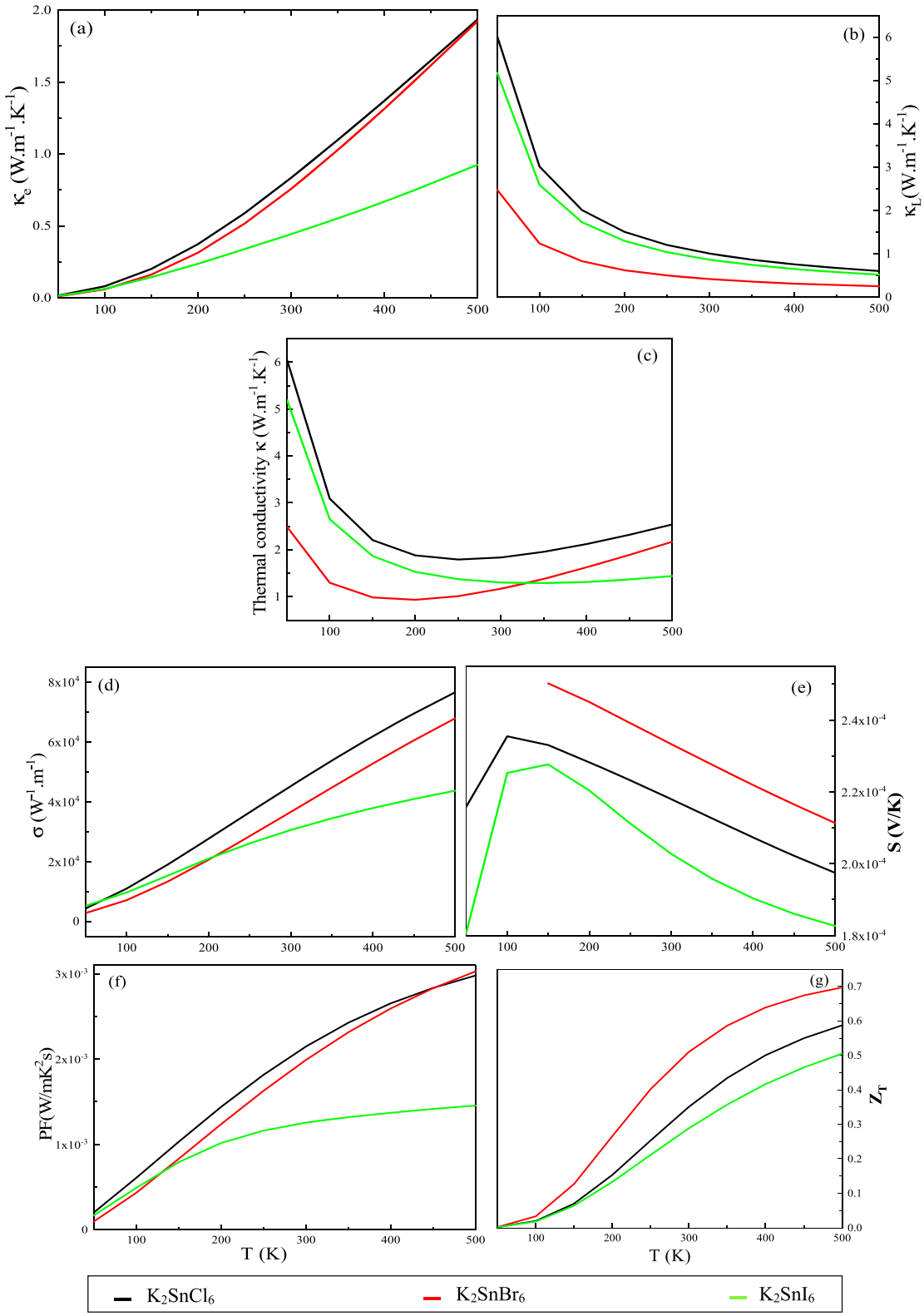


**Figure 6.** The computed $\sigma$, $\kappa_L$, $\kappa_e$, $\kappa$, S, PF, and ZT in terms of temperature, for $K_2SnCl_6$ (X = Cl, Br, I) compounds.

represents the halogens chlorine, bromine, and iodine) by the use of first-principles computations. The present study is centred on the monoclinic phase of these compounds, utilising density functional theory (DFT) and Boltzmann transport theory performed in the wien2k. The purpose of this study is to examine various aspects of these materials.

The band gaps calculated utilising the modified Becke-Johnson (mBJ) potential demonstrate an increasing pattern with regard to electronic properties. Specifically, the band gaps for $K_2SnI_6$, $K_2SnBr_6$, and $K_2SnCl_6$ are recorded as 1.707 eV, 2.581 eV, and 4.126 eV, respectively. The estimated band gaps of $K_2SnX_6$ (X = Cl, Br, and

I) hold great significance for future research because of their near alignment with theoretical values. In addition, it is worth noting that all the compounds under investigation demonstrate direct band gaps except for $K_2SnI_6$, which shows an indirect band gap.

The study of the compounds' optical properties shows that the calculated optical band gaps are the same as the theoretically calculated values found from the band structure calculations. Specifically, $K_2SnI_6$ exhibits a greater intensity in the visible region, which suggests its pronounced absorptive characteristics. The enhanced light absorption capabilities in the visible spectrum exhibited by $K_2SnI_6$ and $K_2SnBr_6$, owing to their narrower band gaps, render them more appropriate for utilisation in solar cell technologies as compared to $K_2SnCl_6$. In addition, it is noteworthy that the refractive index exhibits maximum values at energy levels of 3 eV and 1.9 eV for $K_2SnBr_6$ and $K_2SnI_6$, respectively. This characteristic makes these compounds particularly advantageous for use in solar-related contexts. The compound $K_2SnCl_6$ demonstrates a relatively low refractive index within the visible spectrum, whereas all compounds exhibit a low level of reflection.

When examining the thermoelectric properties, it is observed that substituting bromine or chlorine for iodine results in the creation of broader band gaps, which subsequently enhances electrical conductivity. The thermal conductivity resulting from phonons exhibits a decline as temperature increases, implying a decrease in the transport of heat by phonons. The sign of the Seebeck coefficient indicates the confirmation of *p*-type conductivity in the compounds. Furthermore, it is observed that the power factor is positively correlated with temperature. Specifically, the power factor values for $K_2SnCl_6$ and $K_2SnBr_6$ approach $3 \times 10^{-3}$ W mK$^{-2}$, while for $K_2SnI_6$ it is $1.5 \times 10^{-3}$ W mK$^{-2}$, when the temperature is at 500 K. Additionally, when the temperature reaches 500 K, the aforementioned compounds exhibit peak values of the figure of merit (ZT) at 0.58, 0.69, and 0.50 for $K_2SnCl_6$, K2SnBr$_6$, and $K_2SnI_6$, respectively. The aforementioned findings underscore the prospective utility of these compounds as efficacious materials for thermoelectric applications.

## Acknowledgments

The authors (H Baaziz, T Ghellab, and Z Charifi) would like to thank the general directorate of scientific research and technological development for their financial support during the realisation of this work.

## Data availability statement

The data cannot be made publicly available upon publication because they contain sensitive personal information. The data that support the findings of this study are available upon reasonable request from the authors.

## Declarations

## Conflict of interest

The authors declare no competing interests.

## ORCID iDs

H Baaziz https://orcid.org/0000-0003-4860-2740
Z Charifi https://orcid.org/0000-0003-3875-4716

## References

[1] Rong Y *et al* 2018 Challenges for commercializing perovskite solar cells *Science* **361** eaat8235
[2] Cheng M *et al* 2020 Charge-transport layer engineering in perovskite solar cells *Sci. Bull.* **65** 1237–41
[3] Jia X *et al* 2019 CsPb (I Br1 −)3 solar cells *Sci. Bull.* **64** 1532–9
[4] Kojima A, Teshima K, Shirai Y and Miyasaka T 2009 'Organometal halide perovskites as visible-light sensitizers for photovoltaic cells *J. Am. Chem. Soc.* **131** 6050–1
[5] Zhang Y-Y *et al* 2018 Intrinsic instability of the hybrid halide perovskite semiconductor $CH_3NH_3PbI_3$ * *Chin. Phys. Lett.* **35** 036104
[6] Philippe B *et al* 2015 Chemical and electronic structure characterization of lead halide perovskites and stability behavior under different exposures—a photoelectron spectroscopy investigation *Chem. Mater.* **27** 1720–31
[7] Ju M-G *et al* 2018 Toward eco-friendly and stable perovskite materials for photovoltaics *Joule* **2** 1231–41

[8] Lee B *et al* 2014 Air-stable molecular semiconducting iodosalts for solar cell applications: $Cs_2$ $SnI_6$ as a hole conductor *J. Am. Chem. Soc.* **136** 15379–85
[9] Chen M *et al* 2018 Cesium titanium(IV) bromide thin films based stable lead-free perovskite solar cells *Joule* **2** 558–70
[10] Maughan A E, Ganose A M, Bordelon M M, Miller E M, Scanlon D O and Neilson J R 2016 Defect tolerance to intolerance in the vacancy-ordered double perovskite semiconductors $Cs_2$ $SnI_6$ and $Cs_2$ $TeI_6$ *J. Am. Chem. Soc.* **138** 8453–64
[11] Bhamu K C, Soni A and Sahariya J 2018 Revealing optoelectronic and transport properties of potential perovskites Cs2PdX6 (X = Cl, Br): a probe from density functional theory (DFT) *Sol. Energy* **162** 336–43
[12] Ghrib T *et al* 2021 A new lead free double perovskites K2Ti(Cl/Br)6; a promising materials for optoelectronic and transport properties; probed by DFT *Mater. Chem. Phys.* **264** 124435
[13] Sun Y, Shuai Z and Wang D 2019 Reducing lattice thermal conductivity of the thermoelectric SnSe monolayer: role of phonon–electron coupling *J. Phys. Chem.* C **123** 12001–6
[14] Shi Y, Sturm C and Kleinke H 2019 Chalcogenides as thermoelectric materials *J. Solid State Chem.* **270** 273–9
[15] García G, Palacios P, Cabot A and Wahnón P 2018 Thermoelectric properties of doped-$Cu_3$ $SbSe_4$ compounds: a first-principles insight *Inorg. Chem.* **57** 7321–33
[16] Khan W and Goumri-Said S 2015 Exploring the optoelectronic structure and thermoelectricity of recent photoconductive chalcogenides compounds, $CsCdInQ_3$ (Q = Se, Te) *RSC Adv.* **5** 9455–61
[17] Li G *et al* 2020 Intrinsic mechanical behavior of MgAgSb thermoelectric material: an ab initio study *J. Materiomics* **6** 24–32
[18] Bendahma F, Mana M, Terkhi S, Cherid S, Bestani B and Bentata S 2019 Investigation of high figure of merit in semiconductor XHfGe (X = Ni and Pd) half-Heusler alloys: ab-initio study *Comput. Condens. Matter* **21** e00407
[19] Maccioni M B, Farris R and Fiorentini V 2018 *Ab initio* thermal conductivity of thermoelectric Mg 3 Sb 2 : Evidence for dominant extrinsic effects *Phys. Rev.* B **98** 220301
[20] Mahmood A *et al* 2020 Cation effect on electronic, optical and thermoelectric properties of perovskite oxynitrides: density functional theory *Mater. Sci. Semicond. Process.* **107** 104800
[21] Goh W F and Pickett W E 2020 Topological and thermoelectric properties of double antiperovskite pnictides *J. Phys. Condens. Matter* **32** 345502
[22] Ahmad Mir S and Gupta D C 2021 Understanding the origin of semiconducting ferromagnetic character along with the high figure of merit in Cs2NaMCl6 (M = Cr, Fe) double perovskites *J. Magn. Magn. Mater.* **519** 167431
[23] Li D, Li S, Li X, Yang B and Zhong H 2021 Efficiently synthesized n-type CoSb3 thermoelectric alloys under TGZM effect *Mater. Sci. Semicond. Process.* **123** 105542
[24] Sheng C, Fan D and Liu H 2020 High thermoelectric performance can be achieved in two-dimensional (PbTe)2 layer *Phys. Lett.* A **384** 126044
[25] Shafique A and Shin Y-H 2017 Thermoelectric and phonon transport properties of two-dimensional IV–VI compounds *Sci. Rep.* **7** 506
[26] Haque M A, Kee S, Villalva D R, Ong W and Baran D 2020 Halide perovskites: thermal transport and prospects for thermoelectricity *Adv. Sci.* **7** 1903389
[27] Zhang Y, Yao Q, Qian J, Zhao X, Li D and Mi Q 2020 Thermoelectric properties of all-inorganic perovskite CsSnBr3: a combined experimental and theoretical study *Chem. Phys. Lett.* **754** 137637
[28] Qian X, Gu X and Yang R 2016 Lattice thermal conductivity of organic-inorganic hybrid perovskite $CH_3$ $NH_3$ $PbI_3$ *Appl. Phys. Lett.* **108** 063902
[29] Guo S-D and Wang J-L 2016 Potential thermoelectric materials $CsMI_3$ (M = Sn and Pb) in perovskite structures from first-principles calculations *RSC Adv.* **6** 101552–9
[30] Joshi T K, Pravesh, Sharma G and Verma A S 2020 Investigation of structural, electronic, optical and thermoelectric properties of ethylammonium tin iodide (CH3CH2NH3SnI3): an appropriate hybrid material for photovoltaic application *Mater. Sci. Semicond. Process.* **115** 105111
[31] Wu T and Gao P 2018 Development of perovskite-type materials for thermoelectric application *Materials* **11** 999
[32] Ye T, Wang X, Li X, Yan A Q, Ramakrishna S and Xu J 2017 Ultra-high seebeck coefficient and low thermal conductivity of a centimeter-sized perovskite single crystal acquired by a modified fast growth method *J. Mater. Chem.* C **5** 1255–60
[33] Fedorovskiy A E, Drigo N A and Nazeeruddin M K 2020 The role of goldschmidt's tolerance factor in the formation of $A_2$ $BX_6$ double halide perovskites and its optimal range *Small Methods* **4** 1900426
[34] Ju D *et al* 2019 Tellurium-based double perovskites $A_2$ $TeX_6$ with tunable band gap and long carrier diffusion length for optoelectronic applications *ACS Energy Lett.* **4** 228–34
[35] Ali M A *et al* 2021 Appealing perspectives of structural, electronic, mechanical, and thermoelectric properties of Tl2(Se, Te)Cl6 vacancy-ordered double perovskites *J. Phys. Chem. Solids* **159** 110258
[36] Mahmood Q, Ghrib T, Rached A, Laref A and Kamran M A 2020 Probing of mechanical, optical and thermoelectric characteristics of double perovskites Cs2GeCl/Br6 by DFT method *Mater. Sci. Semicond. Process.* **112** 105009
[37] Huma M *et al* 2021 Physical properties of lead-free double perovskites A2SnI6 (A = Cs, Rb) using ab-initio calculations for solar cell applications *Mater. Sci. Semicond. Process.* **121** 105313
[38] Ullah R, Ali M A, Murtaza G, Khan A and Mahmood A 2020 Ab initio study for the structural, electronic, magnetic, optical, and thermoelectric properties of $K_2$ $OsX_6$ (X = Cl, Br) compounds *Int. J. Energy Res.* **44** 9035–49
[39] Ullah R, Ali M A, Murtaza G, Mahmood A and Ramay S M 2020 The significance of anti-fluorite $Cs_2$ $NbI_6$ via its structural, electronic, magnetic, optical and thermoelectric properties *Int. J. Energy Res.* **44** 10179–91
[40] Higashi T, Syoyama S and Osaki K 1979 Structure of potassium hexabromostannate(IV) at room temperature *Acta Crystallogr.* B **35** 144–6
[41] Boysen H and Hewat A W 1978 A neutron powder investigation of the structural changes in $K_2SnCl_6$ *Acta Crystallogr.* B **34** 1412–8
[42] Schwarz K, Blaha P and Madsen G K H 2002 Electronic structure calculations of solids using the WIEN2k package for material sciences *Comput. Phys. Commun.* **147** 71–6
[43] Perdew J P, Burke K and Ernzerhof M 1996 Generalized gradient approximation made simple *Phys. Rev. Lett.* **77** 3865–8
[44] Perdew J P *et al* 2008 Restoring the density-gradient expansion for exchange in solids and surfaces *Phys. Rev. Lett.* **100** 136406
[45] Becke A D and Johnson E R 2006 A simple effective potential for exchange *J. Chem. Phys.* **124** 221101
[46] Madsen G K H and Singh D J 2006 BoltzTraP. a code for calculating band-structure dependent quantities *Comput. Phys. Commun.* **175** 67–71
[47] Murnaghan F D 1944 The compressibility of media under extreme pressures *Proc. Natl. Acad. Sci* **30** 244–7
[48] Jong U-G, Yu C-J and Kye Y-H 2020 'Computational prediction of structural, electronic, and optical properties and phase stability of double perovskites $K_2$ $SnX_6$ (X = I, Br, Cl) *RSC Adv.* **10** 201–9

[49] Ioffe A F, Stil'bans L S, Iordanishvili E K, Stavitskaya T S, Gelbtuch A and Vineyard G 1959 Semiconductor thermoelements and thermoelectric cooling *Phys. Today* **12** 42
[50] Haque E and Hossain M A 2018 First-principles study of elastic, electronic, thermodynamic, and thermoelectric transport properties of TaCoSn *Results Phys.* **10** 458–65
[51] Slack G A 1973 Nonmetallic crystals with high thermal conductivity *J. Phys. Chem. Solids* **34** 321–35
[52] Otero-de-la-Roza A and Luaña V 2011 Gibbs2: a new version of the quasi-harmonic model code. I. Robust treatment of the static data *Comput. Phys. Commun.* **182** 1708–20
[53] Otero-de-la-Roza A, Abbasi-Pérez D and Luaña V 2011 Gibbs2: a new version of the quasiharmonic model code. II. Models for solid-state thermodynamics, features and implementation *Comput. Phys. Commun.* **182** 2232–48
[54] Zhou Y, Wang J, Luo D, Hu D, Min Y and Xue Q 2022 Recent progress of halide perovskites for thermoelectric application *Nano Energy* **94** 106949